Peer Reviewed Paper openaccess Special Issue on Chemometrics in Hyperspectral Imaging

Concentration monitoring with near infrared chemical imaging in a tableting press

Himmat Dalvi,[a] Clémence Fauteux-Lefebvre,[b] Jean-Maxime Guay,[c] Nicolas Abatzoglou[d] and Ryan Gosselin[e,*]

[a]Department of Chemical & Biotechnological Engineering, Pfizer Industrial Research Chair, Université de Sherbrooke, 2500 boulevard de l'Université, Sherbrooke, Québec, Canada J1K 2R1. ORCID: https://orcid.org/0000-0002-6169-251X
[b]Department of Chemical and Biological Engineering University of Ottawa, 161 Louis Pasteur St, Ottawa, Ontario, Canada K1N 6N5. ORCID: https://orcid.org/0000-0002-0572-250X. E-mail: cfauteux@uottawa.ca
[c]Process Analytical Sciences Group, Pfizer Global Supply, 1025 boulevard Marcel-Laurin, Saint-Laurent, Québec, Canada H4R 1J6
[d]Department of Chemical & Biotechnological Engineering, Pfizer Industrial Research Chair, Université de Sherbrooke, 2500 boulevard de l'Université, Sherbrooke, Québec, Canada J1K 2R1. ORCID: https://orcid.org/0000-0002-9764-4042
[e]Department of Chemical & Biotechnological Engineering, Pfizer Industrial Research Chair, Université de Sherbrooke, 2500 boulevard de l'Université, Sherbrooke, Québec, Canada J1K 2R1. ORCID: https://orcid.org/0000-0002-4607-1141. E-mail: Ryan.Gosselin@Usherbrooke.ca

Monitoring powder potency and homogeneity is important in achieving real-time release testing in a continuous tablet manufacturing operation. If quality related issues are encountered, monitoring powder potency inside a feed frame offers a last opportunity to intervene in the process before tablet compression. Feed frame monitoring methods based on near infrared (NIR) spectroscopy have been increasingly reported in recent years. New process analytical tools with the potential of being deployed alone or in combination with NIR spectroscopy for feed frame monitoring are now available commercially. The present study evaluated the potential of near infrared chemical imaging (NIR CI) for in-line monitoring of a prototype pharmaceutical composition containing ascorbic acid (AA), microcrystalline cellulose and dicalcium phosphate. NIR spectroscopy was the reference method. In-line calibration models based on partial least square regression were developed and validated with a range of AA concentrations. The ability of NIR spectroscopy and NIR CI to predict concentrations in test runs was ascertained both independently and in combination. NIR CI, with a single bandpass filter, predicted AA concentrations—present at commercially relevant concentrations—with acceptable accuracy. Comparative results showed that NIR CI has the potential for in-line monitoring of blend concentrations inside feed frames. In addition to the advantage of increased sample size, it also has the potential to detect segregation inside feed frames.

Keywords: NIR spectroscopy, NIR CI, PAT, feed frame, in-line monitoring

Introduction

Pharmaceutical regulatory authorities require compliance of every manufactured product batch with pre-approved specifications before its release to market. Compliance is crucial for the safety and efficacy of patient medications. Conventionally, batch release takes place after all quality testing of representative samples has been completed, which could lead to considerable lag time and significant costs. Real-time release of pharmaceuticals is becoming possible by taking advantage of recent technological advances as well as recommendations from regulatory agencies for continuous process monitoring.[1] Product and process information collected during manufacturing can ensure that it complies with intended quality stand-

Correspondence
Ryan Gosselin (Ryan.Gosselin@Usherbrooke.ca)

Received: 12 September 2017
Revised: 16 February 2018
Accepted: 20 February 2018
Publication: 5 March 2018
doi: 10.1255/jsi.2018.a5
ISSN: 2040-4565

Citation
H. Dalvi *et al.*, "Concentration monitoring with near infrared chemical imaging in a tableting press", *J. Spectral Imaging* **7,** a5 (2018). https://doi.org/10.1255/jsi.2018.a5

ards. Such information can be obtained by measuring the critical quality attributes (CQAs) of raw materials, in-process materials and critical process parameters (CPPs) during different manufacturing stages. Process analytical technology (PAT) tools enable CPP and CQA measurements in-line, on-line and at-line during the manufacture of different dosage forms, such as tablets, capsules and liquids.[2]

NIR spectroscopy as a PAT tool for tablet manufacturing

Pharmaceutical tablet production involves material handling through a series of steps, including sieving, mixing, particle size enlargement/granulation, drying, compression, sorting and packing.[3] These different operations can elicit significant changes in material attributes which must be monitored to ensure final product quality. Near infrared (NIR) spectroscopy based PAT applications have been developed for monitoring operations such as blending,[4–7] granulation,[8–10] drying[11,12] and continuous mixing followed by compression,[13] coating[14] and end product testing,[14–19] where it has proven to be advantageous over conventional in-process sampling and testing methods.

In addition to these key operations, consistent die-filling is important to meet tablet quality attributes. The feed frame helps maintain constant a supply of materials for die-filling during compression: it is the very last place to access powder just before compression. Powders undergo continuous shearing inside feed frames, which may cause component segregation.[20] From the real-time release testing (RTRt) perspective, if blend concentration is ensured by meeting required specifications inside the feed frame, then monitoring tablet weight alone would be sufficient for tablet assay in RTRt. However, a number of undesirable phenomena occurring inside the feed frame (e.g., material segregation) may impact final product quality.[21] Thus, process compliance inside the feed frame is a must to determine final product quality.

Continuous material movement inside the feed frame evokes significant changes in physical properties (e.g., density) which, in turn, poses a challenge for the development of successful PAT methods for in-line feed frame monitoring.[22] Such powder flow phenomena occurring inside the feed frame, e.g. density variations[23] and segregation,[21] have been explored with NIR spectroscopy. Despite challenges related to sample presentation, NIR spectroscopy has been useful in in-line concentration monitoring inside the feed frame.[23–25]

Near infrared chemical imaging (NIR CI) in feed frame monitoring

Effective sample size is an important parameter for successful in-line feed frame monitoring. In NIR spectroscopy based powder sample testing, it can be estimated with certain parameters, such as NIR beam diameter, its penetration depth and powder density.[26,27] NIR spectroscopy based PAT methods verify content uniformity based on a small blend area (i.e., often a circular expanse 4–6 mm in diameter) illuminated by the NIR beam.[26] Because of low sample scrutiny levels, it is possible for segregation, if present, to remain unnoticed. This limitation may be eliminated by NIR CI, which acquires chemical information over larger sample areas (e.g., 5 × 2 cm) using larger sensor arrays (e.g., 256 × 320 pixels) as compared to NIR spectroscopy probes (e.g. 128 × 1 pixels). In addition, spatial and spectral information could potentially enhance process understanding as well as impart confidence in process data interpretation, e.g., for end-point determination of blending.[28–32] NIR CI based applications developed with the aim of pharmaceutical quality assurance have been successful in analysing the distribution of ingredients in tablets,[33–35] their content uniformity,[36] dissolution rates[37] as well as testing for counterfeit products.[38] To the authors' knowledge, NIR CI for in-line feed frame monitoring has not yet been reported.

The main purpose of the present study is to determine the operational feasibility of NIR CI in a dynamic feed frame environment with a bench-top feed frame set-up. NIR CI, with selected wavelength band filters, gives grey-scale images that could help monitor the concentration and spatial distribution of NIR-active materials. NIR spectroscopy served as a reference method, validating the state of mix and NIR CI results, since it has already been undertaken for feed frame monitoring.[39] Sample volume was estimated both for NIR CI and NIR spectroscopy. NIR data were evaluated for qualitative and quantitative differentiation of powder blends according to various AA concentrations. AA values with NIR CI were compared against NIR spectroscopy and combined NIR spectroscopy/NIR CI data. NIR CI potential to quantify segregation was also assessed. Its capability could constitute a major advancement in feed frame monitoring.

Materials and methods

Materials

All samples in this study consisted of AA (DSM, Jiangsu), microcrystalline cellulose (MCC, Avicel PH 101®, FMC biopolymer) and dicalcium phosphate (DCP, Di tab®, Innophos) at different relative AA concentrations. MCC, DCP and AA particle sizes were 77–156 µm, 150–420 µm and 150–850 µm, respectively. Particle size specifications according to supplier certificates of analysis were: d90 within 77–156 µm for MCC, d80 within 150–425 µm for DCP, d70 within 150–850 µm and d20 above 850 µm for AA. All the materials used in this study were taken from a single lot of the respective materials, thus particle sizes were essentially maintained constant, however, significantly varying particle sizes between different lots of any of the materials may impact performance of calibration model.

Methods

NIR penetration in samples

Sample volume estimation is important to ensure the required level of scrutiny for blend homogeneity.[26] In addition, regulatory specifications of tablet uniformity are dependent on the number of units sampled. Sample volume estimation in feed frame monitoring is necessary to predict tablet uniformity based on feed frame concentrations.

Sample volume could be estimated for each NIR CI and NIR spectroscopy measurement with the following equation:[26]

$$\text{Sample volume} = A \times B \times C \quad (1)$$

where A is the sample area tested by the respective tool, B is NIR penetration depth and C is sample bulk density.

NIR penetration depth inside samples is required to ascertain feed frame sample volume. A modified experimental protocol was set up for this purpose based on the variable layer thickness method proposed by Berntsson *et al.*[27] They reported that sample reflectance increases with increasing powder thickness until the latter reached an optically thick level. Changes in reflectance at different powder thicknesses could be traced to the penetration of NIR radiation into the samples. In the present work, repeated NIR CI at 2 mm and higher thicknesses showed no differences in pixel intensities: thus, this thickness was considered as equal to or greater than that of optically thick samples. Actual NIR penetration was determined by comparing pixel intensities at lower than 2-mm thickness to 2-mm or higher sample thickness.

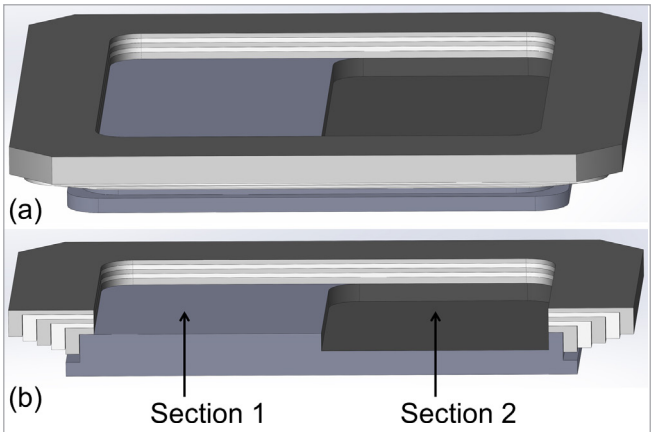

Figure 1. Sample tray: (a) complete view and (b) cross-section.

A plastic tray (Figure 1a) 5 × 4 cm in size was cast and divided into two halves (sections 1 and 2). These two halves were identical except for their depth, which differed by 2 mm (Figure 2b). The purpose of this set-up was to compare pixel intensities acquired from sections 1 and 2. When sufficient powder is placed in the tray, both sections should present similar responses in terms of pixel intensities; if not, the base of the tray will impact the signal of the shallower section (more NIR light will be reflected back to the NIR camera sensor if the light passes through the sample to the reflective surface of the base, thus pixels will have higher intensity).

Tray lids of different thickness (0.5, 0.75, 1.0, 1.5, 2.0 and 2.5 mm) were cast. When no lid was placed on the tray, section 1 had no depth, whereas section 2 was 2 mm deep. Section 1 depth becomes 0.5 mm with the 0.5-mm lid placed on the tray, while it becomes 2.5 mm for section 2. Each time a new lid was placed on the tray, sample material (AA particle size 354–420 µm) was filled in the tray and any excess above the tray lid level was gently scraped off.

Feed frame set-up

This study was conducted in the feed frame of a Manesty Novapress 37-station rotary tablet press. The experimental set-up comprised a fully functional feed frame without actual tablet compression. It helped to mimic powder movement in full-scale tablet manufacturing, but significantly reduced the amount of material required as well as human effort during trials. The feed frame consisted of two counter-rotating wheels (Figure 2a),

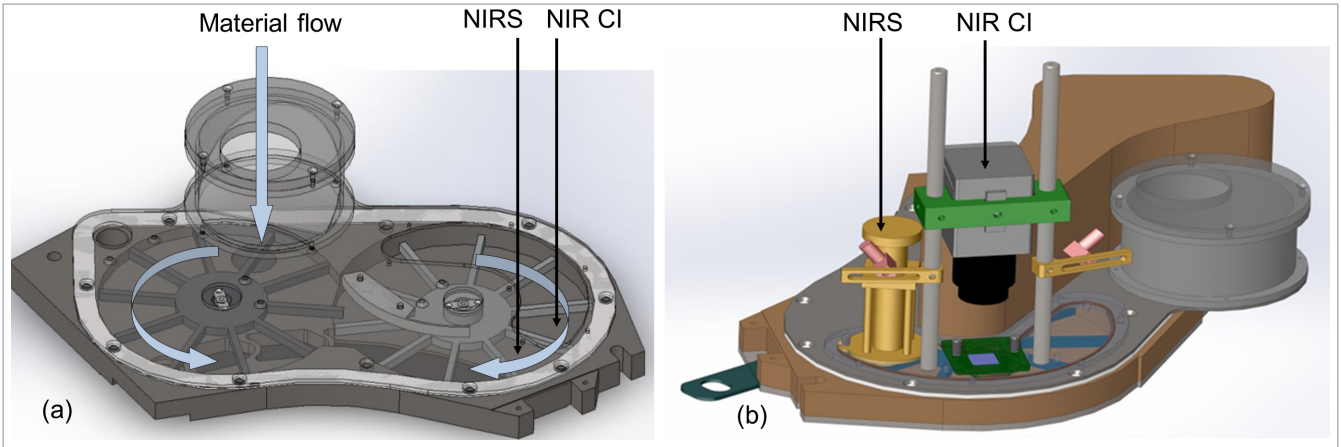

Figure 2. Feed frame set-up: (a) material flow and (b) NIR spectroscopy and NIR CI locations.

each with ten paddles. The second wheel was located slightly lower than the first wheel to facilitate material movement inside the feed frame. The PAT tools for NIR spectroscopy and NIR CI were placed above the second wheel (Figure 2b) just before the point where powder exits the feed frame and enters die cavities for compression.

Data acquisition inside the feed frame

Two data acquisition tools were employed: a NIR probe (MicroNIR 1700, Viavi Solutions, Inc., Milpitas, CA, USA) and a NIR camera (Bobcat 320, Xenics infrared solutions, Leuven, Belgium) with 25-mm infrared lens (Navitar, Rochester, NY, USA). Both tools acquire NIR data in the 900–1700 nm range, as described below.

NIR probe: The NIR probe was equipped with a spectroscope (resolution: 6.2 nm) that discretised the spectrum into 128 levels. The probe's tip was slightly tilted in the direction of material flow, while keeping the observation window (5 × 15 mm) flat, and was mounted on a micrometer. This allowed the measuring tip to precisely touch the powder bed during measurements without reaching the paddle wheel. In this manner, NIR measurements helped to minimise baseline shifts due to powder wave behaviour inside the feed frame, since there was no change in the path-length of the NIR radiation; however, baseline shifts due to changes in powder density caused by moving feed frame paddles were present.

NIR camera: The NIR camera was not equipped with a spectroscope: it integrated all energy levels into a single greyscale image (320 × 256 pixels). However, different wavelength bandpass filters (Spectrogon Inc., Mountain Lakes, NY, USA) were affixed in front of the lens to capture narrow wavelength ranges chosen for specific active ingredients. Filters with wavelength ranges of 1240 ± 40 nm, 1460 ± 11 nm, 1600 ± 63 nm and 1653 ± 19 nm were tested for their suitability to differentiate AA from other components of the powder blend in NIR CI. A suitable filter was expected to selectively allow passage of wavelength ranges absorbed by AA (where MCC and DCP do not show NIR absorbance) to the NIR camera sensor, thus image pixels representing AA would appear darker than the pixels representing other components of the blend. As a result, NIR chemical imaging in the present work refers to a greyscale NIR image captured over a selective NIR wavelength span. The set-up was adapted for proper and constant powder presentation. The movement of the paddles formed large crests and troughs at the surface of the powder (Figure 3a, 3b), impacting image acquisition. As can be observed from the comparison of Figure 3a and 3c, NIR chemical image quality is hampered due to self-shading of material in the presence of a crest and trough pattern caused by the feed frame paddle wheel. A flat insert (2.5 × 5.0 cm) was added to the feed frame surface to constrain these variations in front of the camera to capture the moving powder surface (Figure 3c, 3d). It was positioned 2.5 mm inside the powder whereas the lower tip of the NIR probe was situated at 5 mm inside the powder.

Formulations

Two sets of experiments, each with seven samples (with different AA concentrations), were carried out on two different days. Both experiments analysed the same concentrations, sample volume and blending time. AA

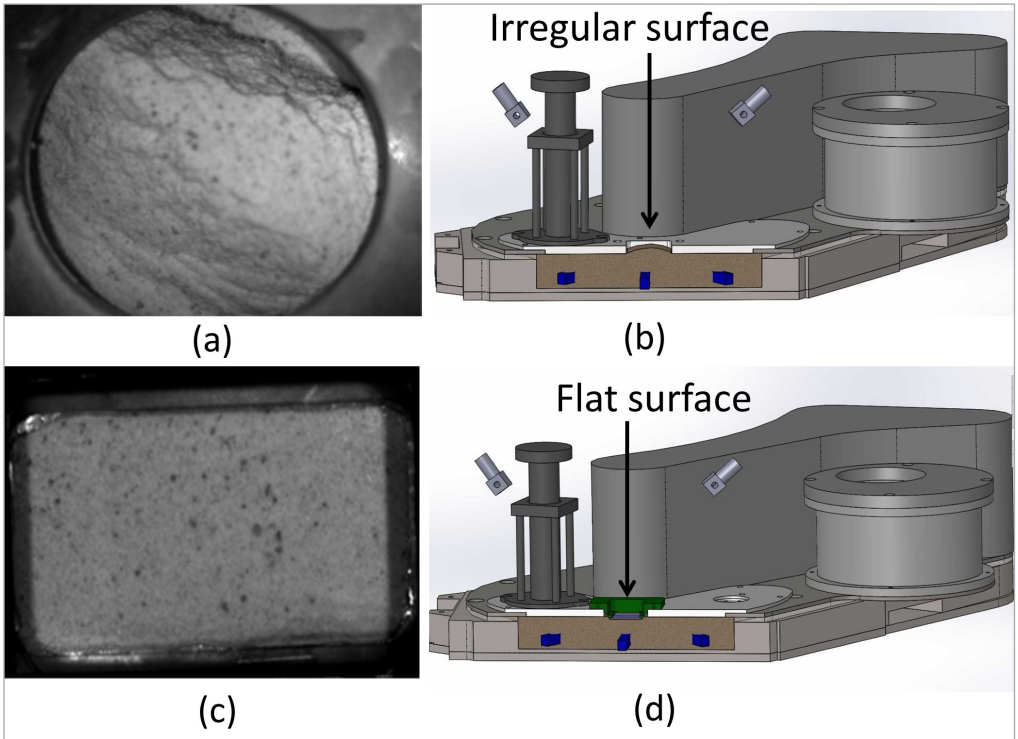

Figure 3. NIR CI inside the feed frame: without flat insert (a: top view, b: schematic vertical cross-section) and with flat surface (c: top view, d: schematic vertical cross-section).

concentrations were increased in a stepwise manner via 3% concentration increments between consecutive blends in order to develop the quantitative model. For the sake of simplicity, the first and second experimental sets will be referred to as trials 1 and 2. The purpose here was to prepare and validate quantitative models in trial 1, and to evaluate them for prediction of similar concentrations in trial 2.

Samples with five different concentrations (0, 3, 6, 9 and 12 %w/w AA) from trial 1 were used for the development of the calibration model based on partial least square (PLS) regression. Performance of PLS calibration model was tested in three ways:

- Test set I (300×76), with 4 and 8 %w/w AA powder samples from trial 1, which represented model applicability for samples from the same trial.
- Test set II (300×76), with 4 and 8 %w/w AA samples from trial 2, represented model applicability to test 1 concentration but in a second trial set.
- Test set III (750×76), with 0, 3, 6, 9 and 12 %w/w AA samples from trial 2, represented model applicability to concentrations as in calibration samples but in a second trial set.

(300 and 700 represent the number of samples, while 76 represents number of histogram bins in NIR CI, for NIR spectroscopy 76 is replaced by 80, i.e. the number of

Table 1. Sample compositions in trials 1 and 2.

Ingredients	Mass concentrations (%w/w)						
	Trial 1—Calibration Trial 2—Test III					Trial 1—Test I Trial 2—Test II	
AA	0.0	3.0	6.0	9.0	12.0	4.0	8.0
MCC	54.5	53.0	51.5	50.0	48.5	52.5	50.5
DCP	45.5	44.0	42.5	41.0	39.5	43.5	41.5

wavelengths.) Table 1 lists the different sample compositions analysed in this study.

Sample quantities were selected on the basis of feed frame working volume, obtained (550.0 g) by adding material slowly inside the closed feed frame until it was full and no more material was accepted inside. Samples were prepared by mixing excipients and AA granules together in a 3-litre V-blender (Patterson Kelley Blend Master, East Stroudsburg, PA, USA) for 10 min. Blending time was kept constant for all samples to ensure uniform blending. The samples were charged and circulated inside the closed feed frame for 10 min at 20 rpm of the paddle wheels. In total, 200 signals (each of NIR spectra and NIR CI) were recorded at a rate of one acquisition per rotation of the paddle wheel.

Data acquisition

NIR spectroscopy

Spectral integration time was 5 ms for NIR spectroscopy signals, with 50 spectra averaged to obtain output signals. An external mechanism was triggered each time to initiate spectral acquisition.

Before acquisition, the NIR probe was calibrated between 0% and 100% reflectance. For the 0% set-up, a NIR spectrum was acquired in the absence of infrared light while for the 100% set-up, a NIR spectrum was recorded by pointing the NIR beam at a 100% reflectance reference. Every raw spectrum (R) acquired during the trials was corrected (C) with the 0% and 100% reflectance standards according to equation 2:

$$C = \frac{R - D}{B - D} \tag{2}$$

where D is 0% reflectance (dark) and B is 100% reflectance reference (bright).

NIR CI

Sample presentation to the camera was properly controlled to ensure image-to-image data comparability. Sample-to-camera distance, optics, illumination and sample surface settings were kept constant. In addition, all NIR images were corrected for NIR source intensity variation over time using a white reference. For this purpose, a white reference was placed across the vertical axis on one corner of the flat insert. A ratio between mean intensity of all the pixels representing this white reference in each respective image and the first image was used to correct the respective image for variation in the NIR light intensity. This ratio was multiplied to all pixel intensities in the NIR chemical image being corrected.

Considering differences in the NIR absorption of AA and other components (MCC, DCP), a 1632–1671-nm filter was selected to capture NIR images since it offered comparatively greater contrast in pixels representing AA and other components (other components reflected more at selected NIR wavelengths).

Data treatment

All NIR spectra and image data obtained from the trials were analysed by in-house MATLAB scripts as well as the PLS Toolbox (Eigenvector Research, Inc., Manson, WA, USA). NIR spectra were evaluated with different pretreatments, such as standard normal variate (SNV), Savitzky–Golay (SG) second derivative, mean centring and scaling to unit variance.

NIR spectra of all individual components, combined other components and composite sample (12% w/w AA) were acquired (Figure 4a). The diffuse reflectance intensity of all ingredients (AA, MCC and DCP) kept on increasing roughly until 1614–1651 nm and then decreased. However, distinct spectral features started to appear only after 1100 nm as the other components (MCC, DCP) absorb less than AA.

Baseline shifts in raw spectra were removed to a significant extent as a result of pretreatments by SNV and SG second derivative (second order polynomial and 15 points). Colour-coded plots of SG second derivative pretreated spectra (Figure 4b) revealed differences in the spectral signature of different samples over the 1100–1590 nm range. As a result, all wavelengths in this spectral range were used in principal component analysis (PCA) and further PLS analysis.

NIR chemical images with a single filter do not contain any spectral information (as in the case of a spectrograph) but provide a 2D representation of the sample as seen over the particular wavelength band allowed by the selected filter. Pixel intensities are influenced by the presence of NIR-active and NIR-non-active material: consequently, the distribution of pixel intensities could quantify content in a spectral format in a way similar to NIR spectroscopy. Consequently, intensities of all pixels in NIR images were expressed in the form of intensity histograms, which classified them into different bins based on their intensity.

Figure 5 depicts the histogram of a greyscale schematic image of the feed frame in which the X-axis

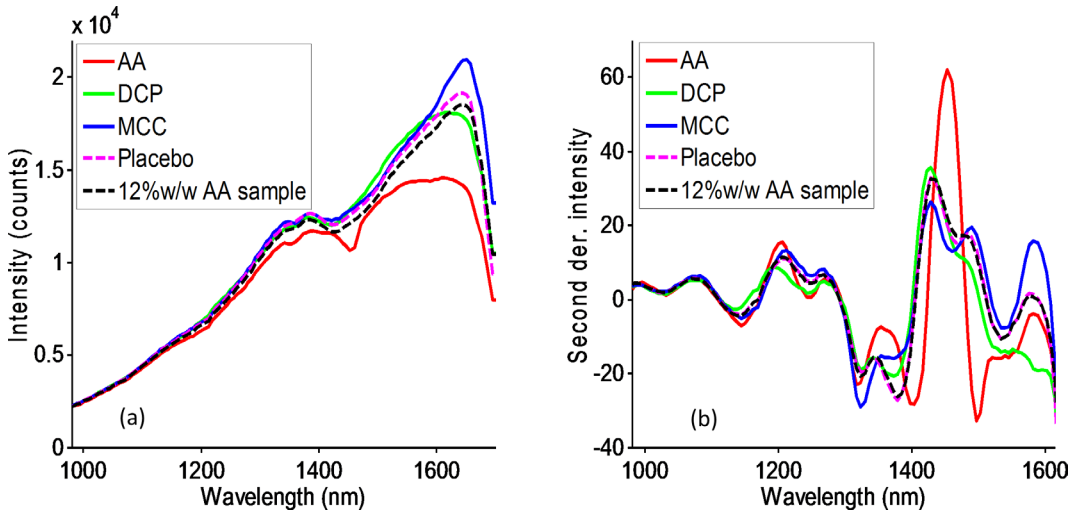

Figure 4. (a) NIR reflectance spectra of individual components and composite samples, (b) SG second derivative pretreated spectra of individual components and composite samples.

represents 8-bit image intensity, and the Y-axis embodies the proportion of pixels in each respective bin. Darker pixels are placed in bins close to origin on the X-axis while brighter pixels are placed away from the origin.

Data analysis by PCA and PLS

PCA and PLS were undertaken for data analysis. Initially, exploratory PCA was conducted to check if individual blend concentrations could be identified by respective signals. Thereafter, the quantitative relationship of NIR CI with respective sample concentrations was evaluated against NIR spectroscopy and the combination of NIR CI with NIR spectroscopy by PLS.

PLS models were statistically compared by R^2 (coefficient of determination in the calibration model), root mean square error of calibration (RMSEC) and root mean square error of cross validation (RMSECV). Ten repeats were used in cross validation. Root mean square error of prediction (RMSEP), mean value and standard deviation of predicted concentrations were compared in tests 1, 2 and 3. In the end, average NIR image of each sample blend and PLS concentration predictions were evaluated in different sections of NIR images.

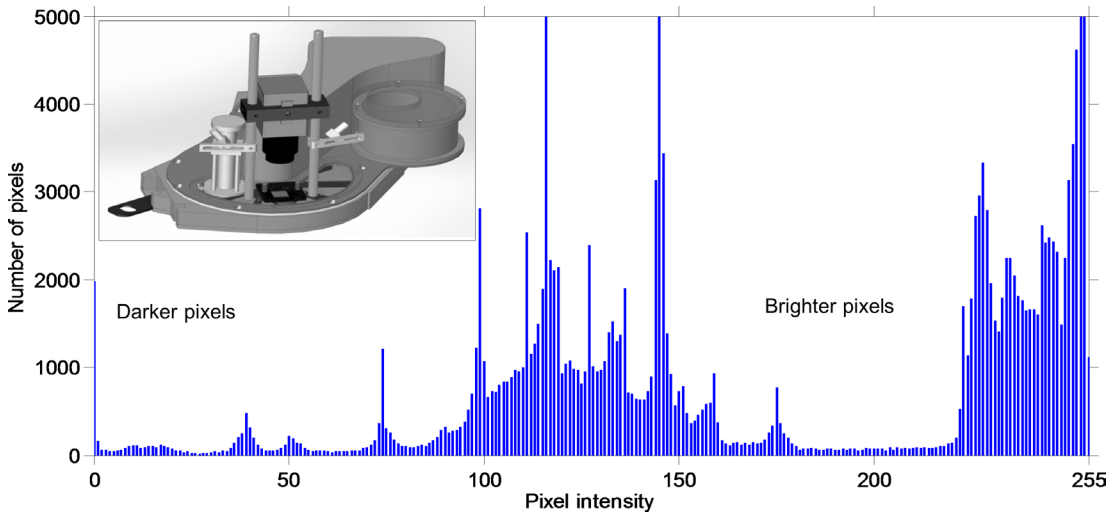

Figure 5. Histogram of a binary image.

Result and discussion

Sample volume

Sample volume was estimated by NIR spectroscopy and NIR CI, starting with the assessment of NIR penetration. In case of NIR spectroscopy, multiple spectra were collected for analysis of each specific thickness sample (90 × 128). Spectral variations among different thickness samples were evaluated by PCA of complete spectra. SNV followed by mean centring was used as a spectral pretreatment to maintain baseline variations caused by different levels of NIR light penetration. Principal component 1 (PC1), which represents 90.19 % of total variance, explained the baseline variations seen among these spectra. PC1 versus sample plots (Figure 6a) showed that PC1 values kept on increasing with increasing sample thickness and later reached a plateau of around 1.5 mm in depth. Since there was no difference in spectra baselines beyond 1.5 mm thickness, it was concluded that NIR penetration in this case was 1.5 mm.

In the case of NIR CI, unpaired *t*-tests of pixel intensities were performed on two tray sections. The null hypothesis was rejected (at alpha value of 0.05) in samples 2.0–0.0 mm, 2.5–0.5 mm and 2.75–0.75 mm thick, but was accepted for all remaining thickness samples (3.0–1.0 mm, 3.5–1.5 mm and 4.0–2.0 mm), indicating that there were no differences in pixel intensities of the two sections with thickness more than 0.75 mm. Thus, it was concluded that NIR penetration in NIR CI was 0.75 mm. Figure 6b depicts NIR images taken at different thickness combinations and corresponding pixel intensity histograms.

Bulk material density was found to be 0.48 g cm^{-3}. Effective sample area was 3.5 × 2.0 cm, as seen in NIR CI. Sample volume estimation was based on Equation (1) for NIR CI and NIR spectroscopy. It was found that sample per image was 252 mg in NIR CI while sample per spectrum was 54 mg in NIR spectroscopy. NIR penetration inside the sample was higher in NIR spectroscopy than in NIR CI, however, sample volume with NIR CI was estimated to be about five times higher than with NIR spectroscopy. As an example, for a 250-mg tablet, each NIR CI would represent a sample equivalent to tablet weight, but five spectra would be required to exemplify the same sample in NIR spectroscopy. Considering the possibility of further increasing flat insert size, sample volume in NIR CI could be adjusted to suitably represent tablet weight greater than 250 mg.

Qualitative NIR spectroscopy analysis

Differentiation between calibration samples was evaluated by NIR spectra collected inside the feed frame. PCA was performed on NIR spectral data to highlight qualitative differences between the different samples. Savitzky–Golay (SG) second derivative, SNV followed by mean centring was used as spectral pretreatment. The PCA score plot illustrated in Figure 7 shows clusters for samples with different concentrations.

PC1 captured 75.36 % of total variance while PC2 captured 10.16 %. PC1 correlated with AA concentrations in samples on the basis of PC1 score versus sample plot. Samples with 0, 3 and 6 % w/w AA were well separated. While still present, the separation between samples of 6, 9 and 12 % w/w was not as clear. However, it showed that with NIR spectroscopy data we can see a difference between the calibration samples. Because of this finding, it seemed reasonable to quantitatively analyse NIR spectroscopy data (discussed above) but, first, differentiation of calibration samples in NIR CI data needs to be done.

Qualitative NIR CI analysis

NIR CI data were converted to histograms before qualitative PCA. Separation of the samples into different groups based on NIR CI data was compared with separation of these blends in NIR spectroscopy data.

Histogram comparison in NIR CI

The histograms of calibration samples in Figure 8 indicate that NIR CI was able to distinguish samples with different AA concentrations.

Two major trends were apparent in the comparative distribution of all histograms, i.e., vertical and horizontal shifts. All histograms were produced from same size images: thus, each histogram was made of the same number of pixels representing the sample. In this scenario, a vertical shift in histograms indicates an overall increase in the number of darker or brighter pixels based on corresponding horizontal shift direction. A horizontal shift to the left suggests an increase in darker pixels, while a shift to the right signposts an increment of brighter pixels which, in turn, respectively correlate with higher and lower AA concentrations in samples.

Histograms of 0 % w/w AA samples are located farthest of all on the right side and have the highest

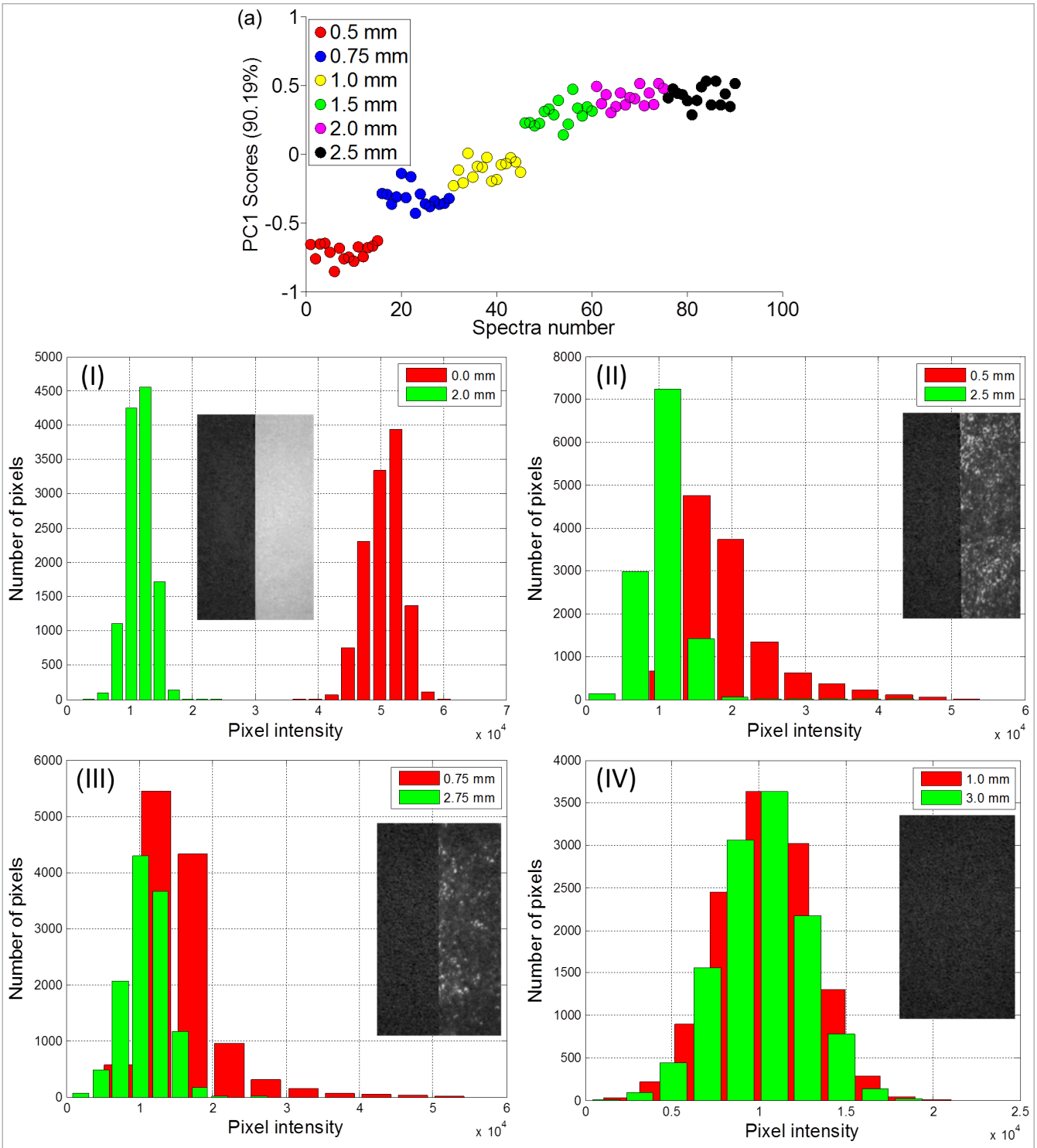

Figure 6. NIR penetration in samples: (a) PCA score plot NIR spectroscopy and (b) NIR CI histogram.

peak height, indicating comparatively narrower distribution of brighter pixels. In contrast, histograms of 12 % w/w samples are located farthest on the left with the lowest peak height, signifies a larger number of darker pixels and comparatively wide pixel distribution.

PCA with NIR CI

The PCA score plot of histogram data (Figure 9) of calibration samples showed differences in the form of distinct cluster points. Mean centring and scaling to unit variance was used for data pretreatment. PC1 captured 80.83 % of total data variance and is correlated with AA concen-

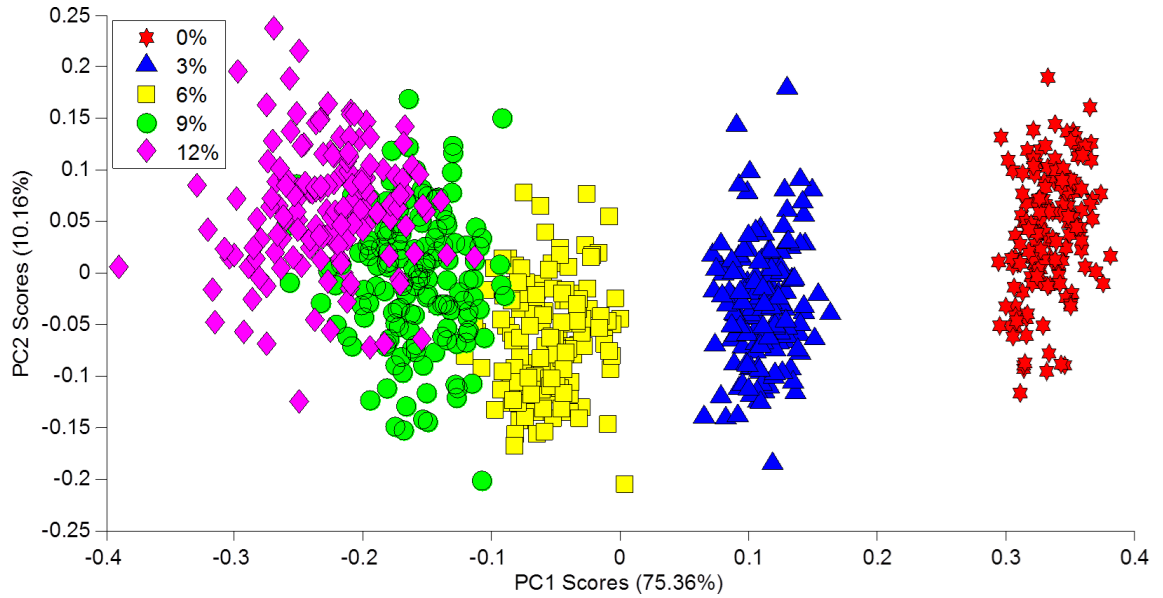

Figure 7. PCA score plots of NIR spectroscopy data (markers with different colour represent % w/w content of AA in respective sample).

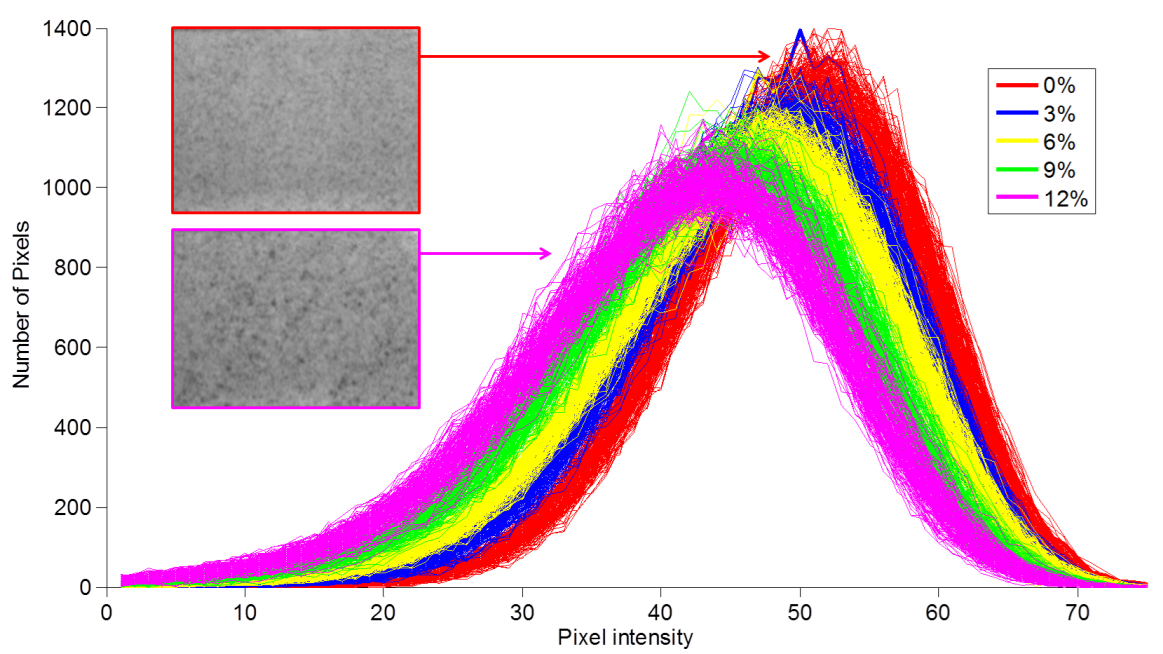

Figure 8. Pixel intensity histograms of calibration samples (colour represents % w/w content of AA in respective sample).

trations in samples. 0%, 3% and 6% w/w samples were very well separated, but there was little overlap in 9% and 12% of them.

In NIR CI, samples with 6, 9 and 12% w/w AA were well separated, while 3 and 6% w/w AA samples were less clearly separated in contrast to NIR spectroscopy data. However, individual observations in all samples show spread around the group cluster in both NIR spectroscopy and NIR CI data. Overall, PCA disclosed that NIR CI was able to represent differences within calibration samples slightly better than NIR spectroscopy because of larger sample size.

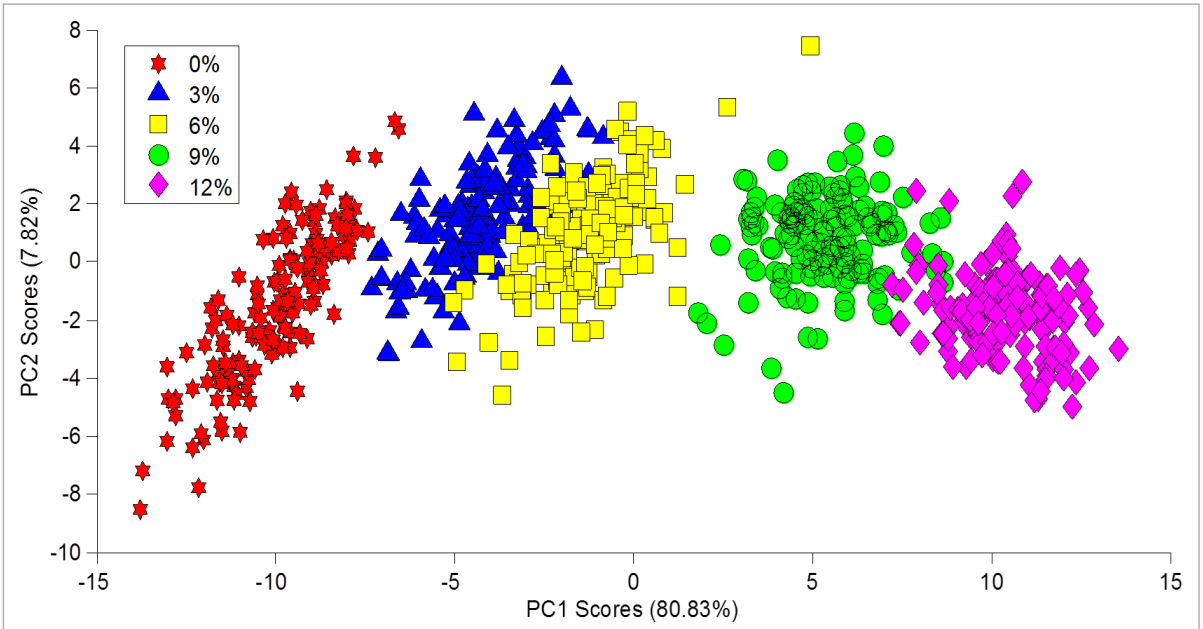

Figure 9. PCA score plot of NIR CI (markers with different colour represent % w/w content of AA in respective sample).

Quantitative analysis

The quantitative relationship between NIR CI (750 × 76) and AA concentration was studied in PLS-based models. PLS-predicted concentrations in NIR CI were compared with NIR spectroscopy (750 × 80) and combined NIR spectroscopy/NIR CI. A combined data matrix (750 × 156) of spatial and spectral information on each sample was obtained by horizontal concatenation of selected NIR spectroscopy/NIR CI data.

NIR CI data were centred and scaled to unit variance before subjecting them to PLS modelling. The PLS model was developed with NIR spectroscopy data, using SNV, SG second derivative (second order polynomial and 15 points) and mean centring pretreatment. For PLS models with combined NIR spectroscopy/NIR CI data, respective data were pretreated individually and then combined. NIR spectroscopy data were pretreated with SNV, SG second derivative (2nd order polynomial with 15 points), centred and scaled to unit variance, while NIR CI data were centred and scaled to unit variance.

Quantitative model comparisons

All PLS models were cross-validated with random subsets during model development. Table 2 summarises the different datasets of PLS model parameters.

Table 2. Summary of PLS performance indicators.

PLS model	Model parameters	PLS model		
		NIR	NIR CI	Combined (NIR/NIR CI)
Calibration	Adjusted R^2	0.96	0.95	0.98
	RMSEC*	0.71	0.81	0.50
	RMSECV*	0.71	0.82	0.51
Test set I	RMSEP*	0.72	0.98	0.53
Test set II	RMSEP*	1.68	1.89	0.75
Test set III	RMSEP*	2.53	2.02	2.18
Number of latent variables		3	3	3

*PLS model errors were expressed in % w/w of AA.

Overall, adjusted R^2 statistics of PLS models based on all three types of datasets (NIR spectroscopy, NIR CI and combined NIR spectroscopy/NIR CI) showed that PLS models fit well with calibration sample data. RMSEC and RMSECV values were higher in NIR CI, lower in NIR spectroscopy and even lower in the combined NIR spectroscopy/NIR CI model. For concentration prediction in trial 1 (test set I), the prediction error of NIR CI was slightly higher than that of NIR spectroscopy and the combined data model. Combining NIR spectroscopy and NIR CI did not improve concentration prediction in unknown samples.

Calibration models with respective datasets (NIR spectroscopy, NIR CI and combined NIR spectroscopy/NIR CI) elicited higher prediction error in trial 2 (test sets II and III) than in trial 1. However, the same calibration models with respective datasets (NIR spectroscopy, NIR CI and combined NIR spectroscopy/NIR CI) predicted well in trial 1 (test set I), which had the same concentration as in test set II. Trials 1 and 2 were performed as separate runs on two different days: thus, higher prediction error could have been the result of variables in data acquisition (such as sample presentation, illumination, NIR source variability, random error) or due to actual variations in the samples. Since data acquisition was carefully controlled and both NIR spectroscopy and NIR CI simultaneously showed higher prediction error, it was likely that unidentified experimental variables caused actual variations (segregation) in trial 2 samples. However, this could be further evaluated on the basis of actual values of predicted concentrations.

Quantitative result comparisons

Unknown sample predictions with NIR CI, NIR spectroscopy and combined NIR spectroscopy/NIR CI data models were compared according to average prediction values and standard deviation. Table 3 summarises the predicted concentrations of unknown samples in test sets I, II and III.

In test set I, average predicted concentrations with PLS models in all three test sets were within the limits of ±1 % w/w. However, standard deviation of predicted concentrations was lower with combined NIR spectroscopy/NIR CI than with individual NIR spectroscopy and NIR CI. Between individual data models, NIR spectroscopy showed lower standard deviation than NIR CI. The distribution of observations in calibration and test samples can be seen in predicted concentrations versus sample plots of the NIR spectroscopy/NIR CI model (Figure 10). Individually, NIR CI showed comparatively wider distribution around measured concentrations than NIR spectroscopy and combined NIR CI-NIR spectroscopy predictions. This may have been due to the combined effect of larger sample area, lower NIR penetration and the comparatively larger particle size of AA granules. Since NIR imaging mostly captured surface distribution, depending on granule size, partial or complete exposure of particles to the surface could possibly have led to differences in consecutive images. It should be noted that the differences were very small and mainly occurred in particular samples. Concentration differences between samples were very well captured at the 1 % w/w level among calibration and test samples.

Table 3. Summary of PLS-predicted concentrations.

Test sets	Measured concentrations of samples (AA % w/w)	Predicted average concentration of sample (1 standard deviation)		
		NIR CI	NIR	Combined (NIR/NIR CI)
I	4.0	3.32 (0.63)	3.84 (0.55)	4.06 (0.36)
	8.0	8.66 (0.77)	8.61 (0.60)	8.44 (0.49)
II	4.0	5.70 (1.10)	6.06 (0.58)	4.69 (0.36)
	8.0	8.20 (0.90)	10.78 (0.73)	7.45 (0.49)
III	0.0	2.10 (1.30)	1.18 (0.55)	3.04 (0.24)
	3.0	5.00 (1.20)	4.69 (0.51)	4.55 (0.41)
	6.0	8.00 (1.20)	8.25 (0.70)	6.05 (0.40)
	9.0	9.00 (1.30)	10.64 (0.77)	8.18 (0.47)
	12.0	11.20 (1.10)	12.06 (0.69)	8.74 (0.46)

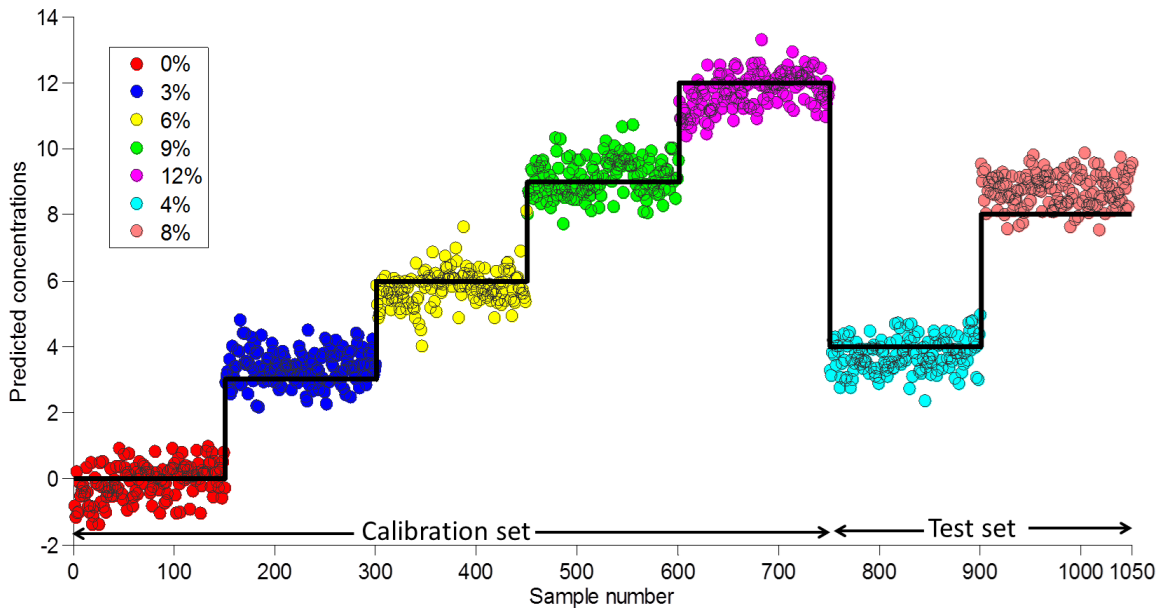

Figure 10. Predicted concentrations versus sample in test I with the combined NIR spectroscopy/NIR CI model (colour represents % w/w content of AA in respective sample).

In test set I, mean values of predicted concentrations showed that the NIR CI based PLS model was in close agreement with the NIR spectroscopy and combined NIR spectroscopy/NIR CI models. One of the major highlights of this work was that NIR CI can monitor feed frame concentrations in capacity at least equal to an already known PAT tool (NIR spectroscopy) for feed frame monitoring. Combination of NIR CI and NIR spectroscopy data does not seem to offer any advantage over the accuracy of the NIR CI and NIR spectroscopy models except for precision (standard deviation) of the predicted values.

In test set II and III concentration predictions, the standard deviation of predicted values followed the same trend (NIR CI > NIR spectroscopy > combined NIR spectroscopy/NIR CI) as in test set I. However, predicted concentrations were not very close to measured values. Average predicted concentration was found to vary in the range of ±2–3 % w/w with all three types of data models.

PLS-predicted concentrations in trial 2 were expected to be close to those in trial 1 considering their exactly identical composition and blending time (i.e., 10 min). However, in the NIR CI data, a few samples (8, 9 and 12 % w/w) were predicted close to measured values while others (4, 0, 3 and 6 % w/w) were not well predicted. Similarly, NIR spectroscopy and combined NIR CI/NIR spectroscopy gave a prediction error of about 2–3 % in all samples, except for 12 % w/w. Since sources of possible variation in NIR spectroscopy data were removed by suitable data pretreatments, prediction bias veered towards other variables, influencing the NIR spectroscopy data. This hints at another possibility: that there could have been actual variations within samples in trial 2, which might lead to variations in predictions. In the present case, tablet compression was not performed subsequently: otherwise, these variations could have been tested by tablet assay. However, NIR CI could still be useful to further probe variations of predicted concentrations in trial 2, since changes in local concentrations could be studied.

Average sample image analysis

The average NIR image of each sample was calculated in both trials 1 and 2. Considering the same mixing time, sample composition, particle size and operation parameters at the feed frame in both these trials, uniform, average images of individual samples were expected. Trial 1 produced uniform average images, but differences in average image intensity were observed in trial 2 (Figure 11a–f). The horizontal axis is essentially parallel to the paddle radius with the left side of the image located near the centre of the paddle wheel.

Average colour-coded imaging established that the pixel intensity of average images changes progressively in samples from lower to higher AA concentrations. At

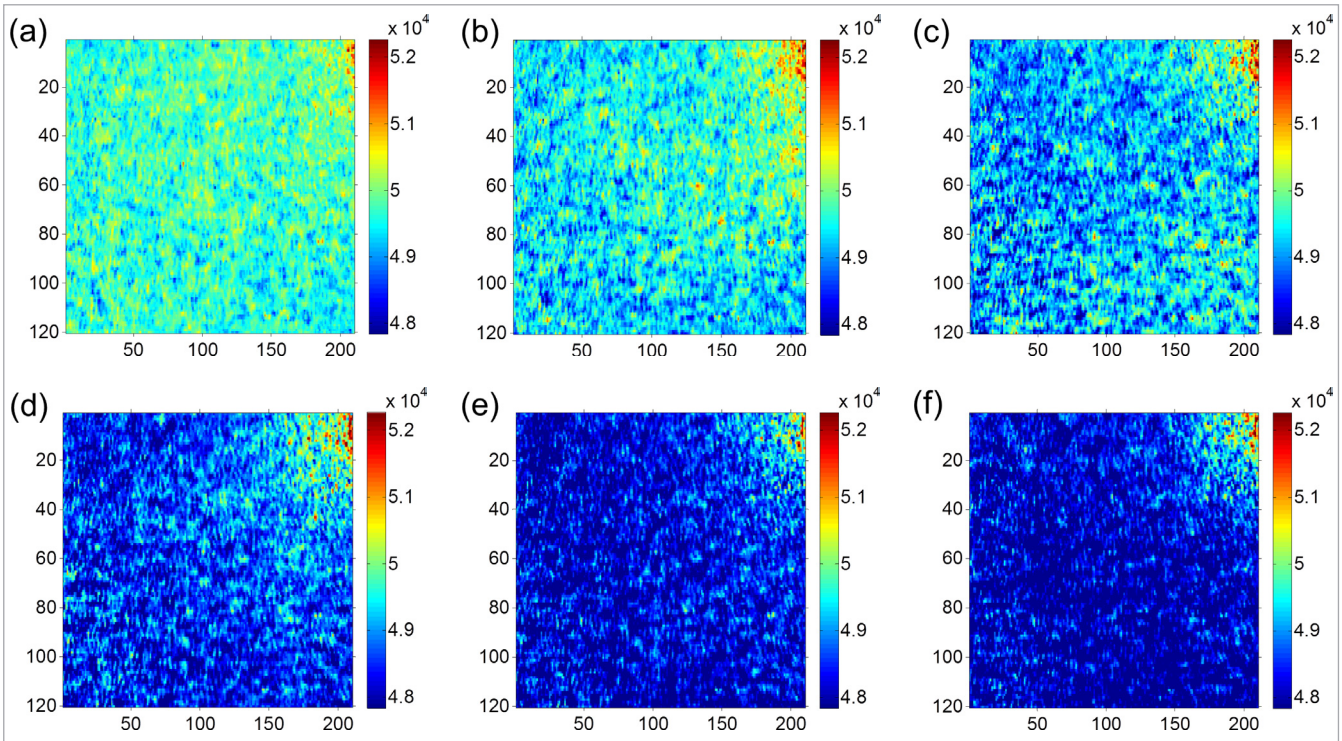

Figure 11. Trial 2 average sample images. a–f represent average image of 3, 4, 6, 8, 9 and 12 % w/w AA samples, respectively. The blue to red colour bar represents decreasing pixel intensity.

the same time, pixels located in the upper-right corner displayed higher intensity compared to the rest of the image. This could potentially indicate lower AA content in the upper-right side of each sample. However, it was merely a qualitative observation, and quantitative analysis was used to confirm local variations in AA concentrations.

Each image was divided into four equal sections (Figure 12), and PLS concentration predictions were made for different image sections.

Here, sections 1 and 3 represent the centre of the feed frame, while sections 2 and 4 represent the circumferential side of feed frame. Table 4 enumerates different

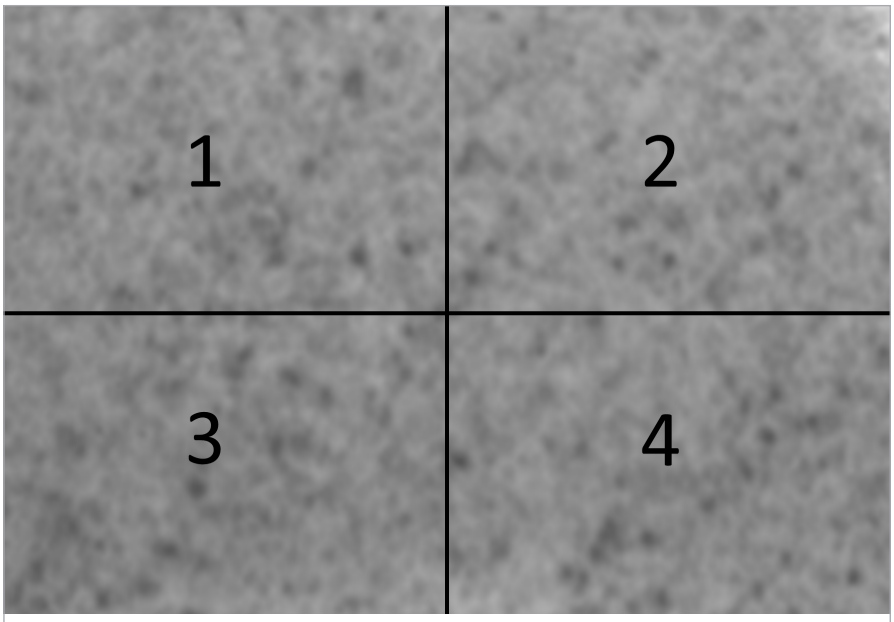

Figure 12. Subsections of the image used in the PLS analysis.

Table 4. Average predicted concentrations in different image sections.

Sample (% w/w)	PLS-predicted sample concentration (1 standard deviation)				
	Section 1	Section 2	Section 3	Section 4	Average
3.0	3.96 (1.62)	0.61 (1.30)	5.28 (1.28)	1.92 (1.17)	2.94 (1.34)
4.0	4.69 (1.39)	1.43 (1.14)	5.22 (1.09)	1.51 (1.11)	3.21 (1.18)
6.0	7.04 (1.50)	2.49 (1.35)	7.50 (1.19)	4.87 (1.15)	5.47 (1.30)
8.0	9.31 (1.56)	5.76 (1.45)	9.53 (1.19)	7.84 (1.37)	8.11 (1.39)
9.0	10.40 (1.45)	6.78 (1.52)	10.65 (1.12)	8.73 (1.21)	9.14 (1.33)
12.0	8.79 (1.52)	7.23 (1.64)	11.61 (1.05)	10.78 (1.19)	9.92 (1.35)

image sections and respective average predicted concentrations.

It was observed that the section representing the upper-right corner of the image (section 2) consistently exhibited lower concentrations in all samples. Section 2 was followed by section 4, showing next lower concentrations. In contrast, the lower-left corner of the image (section 3) presented higher concentrations in all samples, followed by section 1. Standard deviation values in each particular section were also higher, which signified image-to-image variations in samples. This change of local concentrations in different sections further supports the possibility of AA segregation in trial 2.

Conclusion

The main aim of this study was to evaluate the possibility of NIR CI as a PAT tool for in-line feed frame monitoring while using NIR spectroscopy as reference method.

AA concentration predictions with the NIR CI based PLS models were found to be similar to those of the NIR spectroscopy model. NIR CI is better positioned to view concentration modifications over larger sample areas, and different image sections can be analysed separately in the event of localised concentration changes. In the present set-up, sample volume tested by NIR CI was five times higher than NIR spectroscopy. Considering the possibility of adjusting the flat insert size, there is still the prospect of further increasing sample size to meet unit dose samples at feed frame.

An in-line feed frame monitoring system (NIR CI) could help to obtain quantitative as well as visual presentations of powder composition which could be useful for real-time process monitoring by machine operators, e.g., end of material or obstruction of flow, segregation events etc. This study indicates that NIR CI alone or in combination appears to be a promising tool for in-line feed frame monitoring. NIR CI based concentration predictions may prove to be more representative since they gather information from comparatively larger sample area compared to NIR spectroscopy, however, further studies are required to support this hypothesis.

Acknowledgements

The authors acknowledge funding support from the Natural Sciences and Engineering Research Council of Canada RDC Grant with Pfizer Canada Inc. (RDCPJ 449123-13). The technical contributions of Jacques Gagné and Marc Couture (Université de Sherbrooke) are gratefully acknowledged. Special thanks to Pedro Durão for useful discussions and Ovid da Silva for editing this manuscript.

References

1. *Draft Guideline on Real Time Release Testing* (formerly guideline on parametric release). European Medicines Agency (2012).
2. *Guidance for Industry PAT — A Framework for Innovative Pharmaceutical Development, Manufacuring, and Quality Assurance*. US Department of Health and Human Services, Food and Drug Administration, Rockville, MD (2004). http://www.fda.gov/downloads/Drugs/GuidanceComplianceRegulatoryInformation/Guidances/ucm070305.pdf
3. G. Peck, N. Anderson and G. Banker, "Principles of improved tablet production system design", in *Pharmaceutical Dosage Forms-Tablets*, Volume 3,

2nd edition, Ed by J.S. Lieberman and L. Lachman. Marcel Dekker, Inc., New York, pp. 1–2, 4 (1990).

4. P.P. Laponte Gerant, J. Simard and N. Abatzoglou, "Real-time NIR monitoring of a pharmaceutical blending process through multivariate analysis-derived models", *1st WSEAS Int. Conf. Multivar. Anal.* 109 (2008).
5. D. Ely, S. Chamarthy and M.T. Carvajal, "An investigation into low dose blend uniformity and segregation determination using NIR spectroscopy", *Colloid. Surface. A* **288,** 71–76 (2006). doi: https://doi.org/10.1016/j.colsurfa.2006.04.032
6. M. Popo, S. Romero-Torres, C. Conde and R.J. Romañach, "Blend uniformity analysis using stream sampling and near infrared spectroscopy", *AAPS PharmSciTech.* **3,** 61–71 (2002). doi: https://doi.org/10.1208/pt030324
7. O. Scheibelhofer, N. Balak, P.R. Wahl, D.M. Koller, B.J. Glasser and J.G. Khinast, "Monitoring blending of pharmaceutical powders with multipoint NIR spectroscopy", *AAPS PharmSciTech.* **14,** 234–244 (2013). doi: https://doi.org/10.1208/s12249-012-9910-4
8. M. Fonteyne, J. Vercruysse, D.C. Díaz, D. Gildemyn, C. Vervaet, J.P. Remon and T. De Beer, "Real-time assessment of critical quality attributes of a continuous granulation process", *Pharm. Dev. Technol.* **18,** 85–97 (2013). doi: https://doi.org/10.3109/10837450.2011.627869
9. M. Alcalà, M. Blanco, M. Bautista and J.M. González, "On-line monitoring of a granulation process by NIR spectroscopy", *J. Pharm. Sci.* **99,** 336–345 (2010). doi: https://doi.org/10.1002/jps.21818
10. M. Khorasani, J.M. Amigo, P. Bertelsen, C.C. Sun and J. Rantanen, "Process optimization of dry granulation based tableting line: Extracting physical material characteristics from granules, ribbons and tablets using near-IR (NIR) spectroscopic measurement", *Powder Technol.* **300,** 120–125 (2016). doi: https://doi.org/10.1016/j.powtec.2016.03.004
11. M. Fonteyne, J. Arruabarrena, J. De Beer, M. Hellings, T. Van Den Kerkhof, A. Burggraeve, C. Vervaet, J. Paul and T. De Beer, "NIR spectroscopic method for the in-line moisture assessment during drying in a six-segmented fluid bed dryer of a continuous tablet production line: validation of quantifying abilities and uncertainty assessment", *J. Pharm. Biomed. Anal.* **100,** 21–27 (2014). doi: https://doi.org/10.1016/j.jpba.2014.07.012
12. N. Heigl, D.M. Koller, B.J. Glasser, F.J. Muzzio and J.G. Khinast, "Quantitative on-line vs. off-line NIR analysis of fluidized bed drying with consideration of the spectral background", *Eur. J. Pharm. Biopharm.* **85,** 1064–1074 (2013). doi: https://doi.org/10.1016/j.ejpb.2013.09.012
13. K. Jarvinen, W. Hoehe, M. Jarvinen, S. Poutiainen, J. Mikko and S. Borchert, "In-line monitoring of the drug content of powder mixtures and tablets by near-infrared spectroscopy during the continuous direct compression tableting process", *Eur. J. Pharm. Sci.* **48,** 680–688 (2013). doi: https://doi.org/10.1016/j.ejps.2012.12.032
14. J.J. Moes, M.M. Ruijken, E. Gout, H.W. Frijlink and M.I. Ugwoke, "Application of process analytical technology in tablet process development using NIR spectroscopy: blend uniformity, content uniformity and coating thickness measurements", *Int. J. Pharm.* **357,** 108–118 (2008). doi: https://doi.org/10.1016/j.ijpharm.2008.01.062
15. M. Blanco and M. Alcalá, "Content uniformity and tablet hardness testing of intact pharmaceutical tablets by near infrared spectroscopy: a contribution to process analytical technologies", *Anal. Chim. Acta* **557,** 353–359 (2006). doi: https://doi.org/10.1016/j.aca.2005.09.070
16. W. Li, L. Bagnol, M. Berman, R.A. Chiarella and M. Gerber, "Applications of NIR in early stage formulation development. Part II. Content uniformity evaluation of low dose tablets by principal component analysis", *Int. J. Pharm.* **380,** 49–54 (2009). doi: https://doi.org/10.1016/j.ijpharm.2009.06.032
17. I. Tomuţă, R. Iovanov, E. Bodoki and S.E. Leucuţa, "Quantification of Meloxicam and excipients in intact tablets by near infrared spectrometry and chemometry", *Farmacia* **58,** 559 (2010). http://bit.ly/2oKBzJg
18. H. Tanabe, K. Otsuka and M. Otsuka, "Theoretical analysis of tablet hardness prediction using chemoinformetric near-infrared spectroscopy", *Anal. Sci.* **23,** 857–862 (2007). doi: https://doi.org/10.2116/analsci.23.857
19. P. Pawar, Y. Wang, S. Keyvan, G. Callegari, A. Cuitino and F. Muzzio, "Enabling real time release testing by NIR prediction of dissolution of tablets made by continuous direct compression", *Int. J. Pharm.* **512,** 96–107 (2016). https://doi.org/10.1016/j.ijpharm.2016.08.033

20. M.O. Daniel, F.J. Muzzio and R. Méndez, "Particle size segregation promoted by powder flow in confined space: the die filling process case", *Powder Technol.* **262,** 215–222 (2014). doi: https://doi.org/10.1016/j.powtec.2014.04.023

21. P.R. Wahl, G. Fruhmann, S. Sacher, G. Straka, S. Sowinski and J.G. Khinast, "PAT for tableting: inline monitoring of API and excipients via NIR spectroscopy", *Eur. J. Pharm. Biopharm.* **87,** 271–278 (2014). doi: https://doi.org/10.1016/j.ejpb.2014.03.021

22. Y. Liu and D. Blackwood, "Sample presentation in rotary tablet press feed frame monitoring by near infrared spectroscopy", *Am. Pharm. Rev.* **15,** 1 (2012).

23. D. Mateo-Ortiz, Y. Colon, R.J. Romanach and R. Mendez, "Analysis of powder phenomena inside a Fette 3090 feed frame using in-line NIR spectroscopy", *J. Pharm. Biomed. Anal.* **100,** 40–49 (2014). doi: https://doi.org/10.1016/j.jpba.2014.07.014

24. H.W. Ward, D.O. Blackwood, M. Polizzi and H. Clarke, "Monitoring blend potency in a tablet press feed frame using near infrared spectroscopy", *J. Pharm. Biomed. Anal.* **80,** 18–23 (2013). doi: https://doi.org/10.1016/j.jpba.2013.02.008

25. S. Šašić, D. Blackwood, A. Liu, H.W. Ward and H. Clarke, "Detailed analysis of the online near-infrared spectra of pharmaceutical blend in a rotary tablet press feed frame", *J. Pharm. Biomed. Anal.* **103,** 73–79 (2015). doi: https://doi.org/10.1016/j.jpba.2014.11.008

26. H. Wu, M. Tawakkul, M. White and M.A. Khan, "Quality-by-design (QbD): an integrated multivariate approach for the component quantification in powder blends", *Int. J. Pharm.* **372,** 39–48 (2009). doi: https://doi.org/10.1016/j.ijpharm.2009.01.002

27. O. Berntsson, T. Burger, S. Folestad, L. Danielsson, J. Kuhn and J. Fricke, "Effective sample size in diffuse reflectance near-IR spectrometry", *Anal. Chem.* **71,** 617–623 (1999). doi: https://doi.org/10.1021/ac980652u

28. A.S. El-Hagrasy, H.R. Morris, F. D'Amico, R.A. Lodder and J.K. Drennen, "Near-infrared spectroscopy and imaging for the monitoring of powder blend homogeneity", *J. Pharm. Sci.* **90,** 1298–1307 (2001). doi: https://doi.org/10.1002/jps.1082

29. H. Ma and C. Anderson, "Characterization of pharmaceutical powder blends by NIR chemical imaging", *J. Pharm. Sci.* **97,** 3305–3320 (2008). doi: https://doi.org/10.1002/jps.21230

30. W. Li, A. Woldu, R. Kelly, J. McCool, R. Bruce, H. Rasmussen, J. Cunningham and D. Winstead, "Measurement of drug agglomerates in powder blending simulation samples by near infrared chemical imaging", *Int. J. Pharm.* **350,** 369–373 (2008). doi: https://doi.org/10.1016/j.ijpharm.2007.08.055

31. K. Murayama, D. Ishikawa, T. Genkawa, H. Sugino, M. Komiyama and Y. Ozaki, "Image monitoring of pharmaceutical blending processes and determination of an end point by using a portable near-infrared imaging device based on a polychromator type near infrared spectrometer with a high speed and high resolution photo diode array detector", *Molecules* **20,** 4007–4019 (2015). doi: https://doi.org/10.3390/molecules20034007

32. Z. Wu, O. Tao, X. Dai, M. Du, X. Shi and Y. Qiao, "Monitoring of a pharmaceutical blending process using near infrared chemical imaging", *Vib. Spectrosc.* **63,** 371–379 (2012). doi: https://doi.org/10.1016/j.vibspec.2012.09.001

33. R.C. Lyon, D.S. Lester, E.N. Lewis, E. Lee, L.X. Yu, E.H. Jefferson and A.S. Hussain, "Near-infrared spectral imaging for quality assurance of pharmaceutical products: analysis of tablets to assess powder blend homogeneity", *AAPS PharmSciTech.* **3,** 1–15 (2002). doi: https://doi.org/10.1007/BF02830615

34. J.M. Amigo and C. Ravn, "Direct quantification and distribution assessment of major and minor components in pharmaceutical tablets by NIR-chemical imaging", *Eur. J. Pharm. Sci.* **37,** 76–82 (2009). doi: https://doi.org/10.1016/j.ejps.2009.01.001

35. Z. Wu, O. Tao, W. Cheng, L. Yu, X. Shi and Y. Qiao, "Visualizing excipient composition and homogeneity of compound liquorice tablets by near-infrared chemical imaging", *Spectrochim. Acta A* **86,** 631–636 (2012). doi: https://doi.org/10.1016/j.saa.2011.10.030

36. C. Gendrin, Y. Roggo and C. Collet, "Content uniformity of pharmaceutical solid dosage forms by near infrared hyperspectral imaging: a feasibility study", *Talanta* **73,** 733–741 (2007). doi: https://doi.org/10.1016/j.talanta.2007.04.054

37. K. Yekpe, N. Abatzoglou, B. Bataille, R. Gosselin, T. Sharkawi, J. Simard and A. Cournoyer, "Predicting the dissolution behavior of pharmaceutical tablets with NIR chemical imaging", *Int. J. Pharm.* **486,** 242–251 (2015). doi: https://doi.org/10.1016/j.ijpharm.2015.03.060

38. J. Dubois, J.C. Wolff, J.K. Warrack, J. Schoppelrei and E.N. Lewis, "NIR chemical imaging for counterfeit pharmaceutical products analysis", *Spectroscopy* **22,** 40 (2007).

39. R. Gosselin, P. Durão, N. Abatzoglou and J. Guay, "Monitoring the concentration of flowing pharmaceutical powders in a tableting feed frame", *Pharm. Dev. Technol.* **22,** 699–705 (2017). doi: https://doi.org/10.3109/10837450.2015.1102278